Journal of Materials Chemistry A

Accepted Manuscript

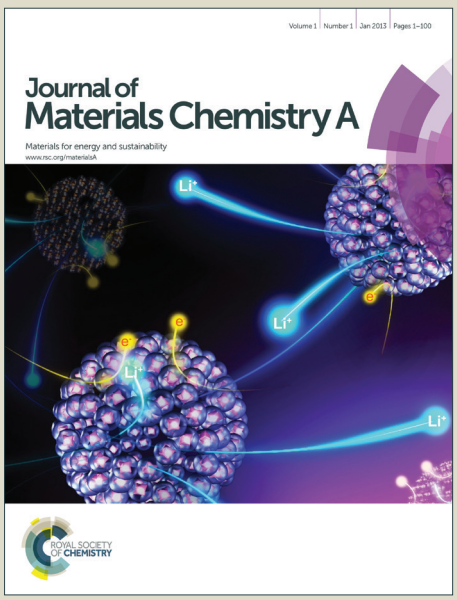

ROYAL SOCIETY OF CHEMISTRY

www.rsc.org/materialsA

Journal of Materials Chemistry A

Journal of Materials Chemistry A

Dynamic Article Links ►

Cite this: DOI: 10.1039/c0xx00000x

Paper

www.rsc.org/xxxxxx

Synthesis and Properties of Silicon/Magnesium Silicon Nitride Diatom Frustule Replicas

Ivar Andre Ødegård[a], Julien Romann[a], Anita Fossdal[b], Arne Røyset[b] and Gabriella Tranell[a,*]

Received (in XXX, XXX) Xth XXXXXXXXX 20XX, Accepted Xth XXXXXXXXX 20XX

DOI: 10.1039/b000000x

The elaboration of nanostructures including both functional materials and functional morphology is a crucial scientific and technological challenge. In this work diatom frustule replicas mainly consisting of magnesium silicon nitride and nanocrystalline silicon have been obtained by simultaneous metallothermic reduction and nitriding of silica diatom frustules at 800 °C. The frustule replicas retained most of the complex nanoporous structure from the original frustules in the conversion. The optical scattering, transmittance and luminescence properties of the replicas have been investigated. Luminescence was observed and attributed to the presence of silicon nanocrystals. Wavelength dependent diffraction of light was observed in bio-silica frustules but not in frustule replicas, this was attributed to surface coarsening of the replicas during reaction. Light transmittance was found to be lower in frustule replicas and was consistent with absorption of light by Si nanocrystals.

Introduction

Background

With an ever increasing role of nanotechnology in everyday life, science is looking towards nature for inspiration, as its complexity is often observed as biosynthesized nanostructures. One of the most well-known examples of complex biological nanostructures is the nanoporous bio-silica shell (frustule) synthesized by diatoms, a major group of single celled algae found in both freshwater and marine environments. Diatom frustules consist of several patterned, often layered, nanoporous structures, with pores ranging from tens to hundreds of nanometers.[1-4] Due to their complex nanoscale morphology, frustules are an excellent example of naturally occurring light harvesting photonic bio-structures.[5-8] In an effort to take advantage of the different properties emerging from such complex nanostructures, diatom frustules have been investigated as templates or substrates for the production of optical biosensors, gas sensors and solar cell substrates.[8-11] Previous works have investigated several ways to characterize and modify the structural, chemical, and optical properties of frustules.[2, 5-8, 12-19] Three dimensional (3D) frustule replicas made of silicon [13, 14], titania [20], barium titanate [21], magnesia [20, 21] and boron nitride [22], respectively, have been obtained by various methods. The possibility of forming silicon nitride frustules replicas has also been briefly mentioned, but without providing any experimental procedure or result.[23] Due to the excellent conservation of structural features by metallothermic reduction of frustules [13-15], the synthesis of nitride containing materials using this method was investigated.[24] In an effort to add new properties to the optical properties arising from the complex frustule morphology, magnesium silicon nitride ($MgSiN_2$) would be an interesting replacement material. Indeed, combining the light harvesting properties of frustules with the luminescent properties of doped $MgSiN_2$ has great potential in solar cell and light emitting diode (LED) technology due to emission of visible light upon illumination by near ultraviolet light (UV) and blue light.[25, 26] Moreover, $MgSiN_2$ exhibits good thermal conductivity, high electrical resistance, high strength, good fracture toughness and high hardness.[27] In this work simultaneous metallothermic reduction and nitriding of diatom frustules was hence attempted in an effort to synthesize 3D diatom frustule replicas showing high concentrations of $MgSiN_2$ while conserving the multi-scaled morphology of the frustules. We also demonstrate luminescence in undoped $MgSiN_2$, consistent with the presence of nanocrystalline silicon.

Experimental

Method and Materials

The metallothermic reduction of silica relies on a self-sustaining reaction obtained by heating silica mixed with a metallic reactant (typically magnesium or aluminium) showing enough difference in chemical potential.[28] Magnesiothermic reduction was chosen to reduce the required temperature for formation of $MgSiN_2$, since significant changes to the frustules morphology have been observed above 800 °C.[29] In order to initiate nitride formation, an atmosphere of nitrogen (N_2) or ammonia (NH_3) must be present during the metallothermic reduction.[27, 30] This can be achieved by passing gaseous N_2 or NH_3 through a reactor, as during

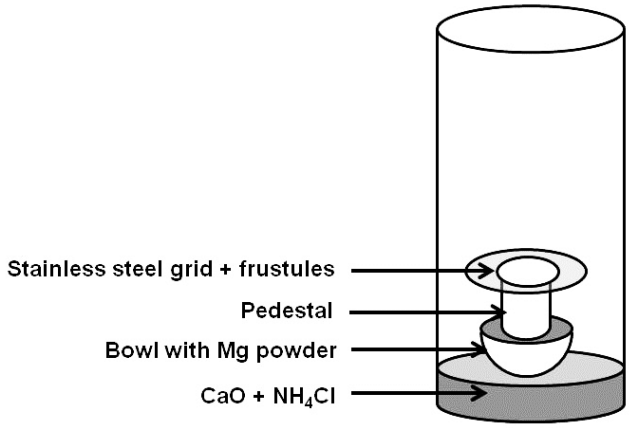

Fig.1 Scheme of the reactor used for the simultaneous metallothermic reduction and nitriding of diatom frustules.

conventional nitriding.[31] Ammonia can also be generated in situ by thermal decomposition (T > 338 °C) of an ammonium salt such as ammonium chloride (NH_4Cl), yielding ammonia and hydrochloric acid.[32] In this work, a locally (to Trondheim, Norway, 63°29'N, 10°15'E) occurring diatom species, *Coscinodiscus centralis* (*C.centralis*), was chosen as the starting point for conversion. *C.centralis* is a centric diatom with an overall diameter ranging from 100 to 300 µm and is frequently encountered along the Norwegian coast.[33] The abundance of this species and its large size compared to other species makes it an interesting choice for experimental work. Frustules biosynthesized by *C. centralis* diatoms are made of different assembled parts: two opposing valves joined together by girdle bands. The combined metallothermic reduction and nitriding process was performed using a custom made stainless steel reactor chamber. A scheme of the synthesis setup is presented in **Fig. 1**. To remove the organic part of the diatom, a peroxide/acid-based cleaning method was applied before the experiments.[34] In order to ensure complete removal of remaining organic residues withstanding the original cleaning procedure, diatom frustules were also heated at 650 °C for 20 min. in a muffle furnace (Bulten Kanthal Super Rapid High Temperature Furnace). The frustules were subsequently cooled to room temperature before being weighed out along with magnesium powder, calcium oxide and ammonium chloride in excess, according to equations 1-4:

Generation of ammonia by thermal decomposition of ammonium chloride mixed with calcium oxide:

$$2NH_4Cl_{(s)} + CaO_{(s)} \rightarrow 2NH_{3(g)} + CaCl_{2(s)} + H_2O_{(g)} \quad (1)$$

Water vapor removal by reaction with magnesium powder:

$$Mg_{(s)} + H_2O_{(g)} \rightarrow MgO_{(s)} + H_{2(g)} \quad (2)$$

Thermal dissociation of ammonia:

$$2NH_{3(g)} \rightarrow N_{2(g)} + 3H_{2(g)} \quad (3)$$

Formation of magnesium silicon nitride:

$$SiO_{2(s)} + 3Mg_{(g)} + 2NH_{3(g)} \rightarrow MgSiN_{2(s)} + 2MgO_{(s)} + 3H_{2(g)} \quad (4)$$

The reactants were then transferred to the steel reactor in a glove box under argon atmosphere. The frustules were transferred to a stainless steel grid and placed on top of a hollow pedestal to create a space between the respective reactants. This space ensured only vapors would be responsible for the various reactions. The reactor was then sealed and taken out of the glove box before being transferred to a muffle furnace and heated to 800 °C at a rate of 20 °C/min. After a holding time of 2 hours at 800 °C, the furnace with reactor inside was cooled down naturally (50 min.), the reactor extracted and opened in ambient atmosphere before extraction of the content. The obtained frustule replicas were immersed in a solution of hydrochloric acid (1M) and ethanol for 30 minutes, rinsed repeatedly in distilled water and in acetone, and finally dried. This was done to ensure that no solvents were carried along during characterization and analysis.

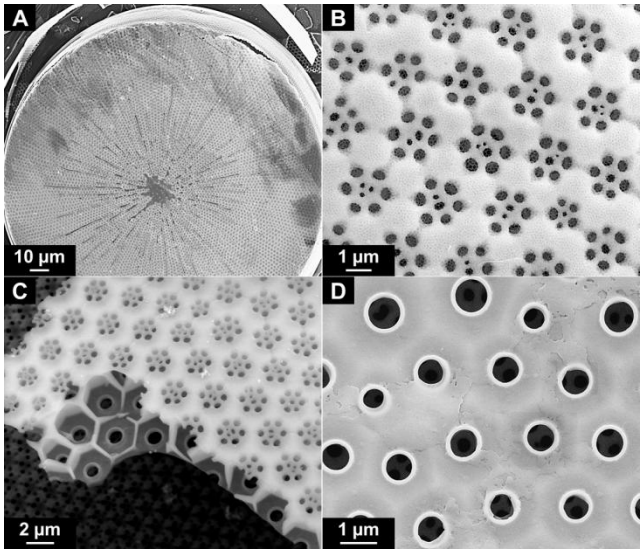

Fig.2 SEM images showing the structure of a *BSi*-frustule valve. Single valve (A); cribrum (B); cracked valve where the cribrum, the areola and the foramen can be observed (C); foramen (D).

Characterization of Starting Material and Product

Both unreacted bio-silica frustules (*BSi*-frutules) and obtained $MgSiN_2$ frustule replicas (*MSN*-frustules) were characterized by low vacuum field effect scanning electron microscopy (LVFESEM, Zeiss Supra 55 VP) at 10 keV, by energy dispersive X-ray spectroscopy (EDS, EDAX Advanced Microanalysis Solutions) at 10 keV and by X-ray diffraction (XRD) using a Bragg–Brentano type diffractometer (Bruker D8 Focus) with a Cu Kα source of radiation. Rietveld analysis, using Topas 4.2 software, of the XRD data was subsequently carried out to evaluate the relative quantities of phases in the reaction products. The background was fitted using a 5th order Chebychev polynomial, and the 20-80° 2θ range was fitted. Optical transmission and luminescence experiments were carried out with a hyperspectral microscope (Applied Spectral Imaging) with 5 nm spectral resolution and equipped with a 10x objective. Optical scattering and diffraction were characterized with a spectrophotogoniometer (LightTec REFLET 180) and micro-Raman imaging (Renishaw InVia) was performed with 532 nm excitation.

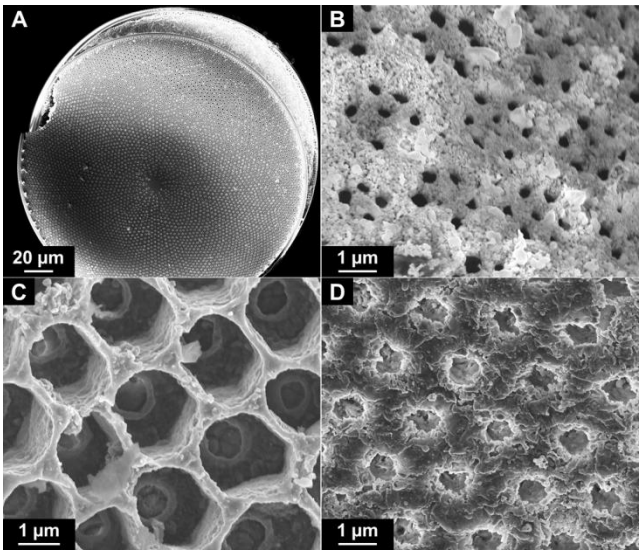

Fig.3 SEM images showing the structure of a *MSN*-frustule valve. Two overlapping valves (A); cribrum (B); areola (C); foramen (D).

Results and discussion

Composition and crystal structure of *BSi* frustules

The porous structure of a *BSi*-frustule valve is presented in **Fig. 2**. The external layer of the valve, called cribrum (**Fig. 2**B), shows a structure of flower-like porous patterns with hexagonal symmetry. The pores of the cribrum are divided into smaller nano pores by thin silica branches. The areola (**Fig. 2C**), located just beneath the cribrum, features a honeycomb structure of bio-silica walls perpendicular to the cribrum. Each flower-like pattern of the cribrum is centered above a hexagonal cavity defined by the structure of the areola. Finally, the foramen (**Fig. 2**D) defines the inner side of the frustule valve and features a hexagonal array of circular pores. Each pore of the foramen is centered with both a hexagonal cavity of the areola and a flower-like pattern of the cribrum. The EDS spectrum of a *BSi*-frustule is presented in **Fig. 4**A, and is consistent with silica (SiO_2) frustules. The XRD diffractogram of *BSi*-frustules is given in **Fig. 5**A. The diffraction peaks could not be unequivocally assigned to silica phases. The peak at 26.5° corresponds well with the main quartz peak (011), however all other quartz peaks are absent. Absence of selected reflections for powder X-ray diffraction analysis is often seen in cases of preferred orientation of highly oriented crystallites, but there is no evidence that would suggest such preferred orientation in this case. The presence of amorphous material, presumably mainly silica, is however clearly evident, so it is considered most likely that the diffraction peaks are due to the presence of organic compounds or impurities.

Structure of *MSN* sample

Two overlapping *MSN*-frustule valves are observed in **Fig. 3**A. Their overall structural integrity appears to be well conserved compared to the *BSi*-frustule valve shown in **Fig. 2**A. The cribrum layer of a *MSN*-frustule is observed in **Fig. 3**B. The surface of the valve has coarsened and the thin branches inside the pores have disappeared, but the typical flower-like porous pattern is retained. An *MSN*-frustule valve after stripping of the cribrum layer, leaves its areola clearly visible in **Fig. 3**C.

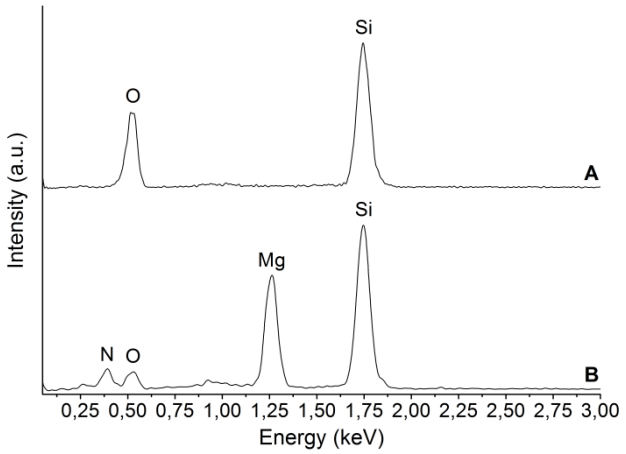

Fig.4 EDS spectra of respectively a *BSi*-frustule (A) and a *MSN*-frustule (B).

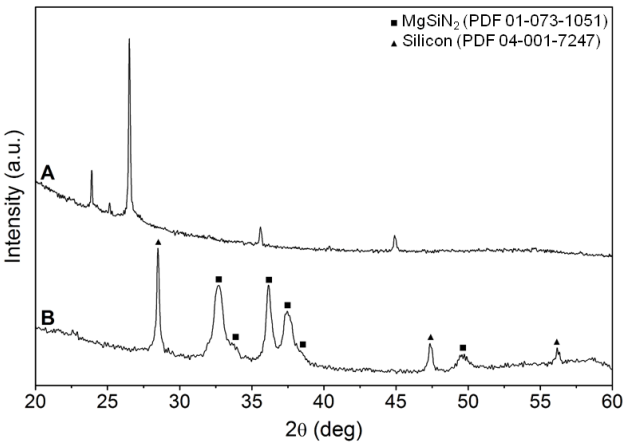

Fig.5 XRD diffractograms of respectively *BSi*-frustules (A) and *MSN*-frustules (B).

The morphology of the areola layer is well conserved as compared to before any chemical transformation (*cf.* **Fig. 2**B). However, similarly to what is observed for the cribrum layer, a significant surface coarsening has taken place. This coarsening was likely caused by sintering occurring during the metallothermic reduction and nitriding reactions.[35, 36] **Fig. 3**D shows the foramen of a *MSN*-frustule valve. Despite partial sintering, the porous pattern of this layer appears to be retained. However, the surface coarsening is very pronounced. This surface coarsening is observed in all parts of the frustule, which indicates that the sintering occurs evenly throughout the structure.

Composition and crystal structure of *MSN* sample

The main elemental constituents of the *MSN*-frustules appear to be silicon, magnesium, nitrogen and oxygen (*cf.* **Fig. 4**B). For the *MSN* frustules, a concentration of nitrogen is indicative of nitride formation. The presence of oxygen suggests that some unreacted silica remains after simultaneous metallothermic reduction, nitriding and cleaning. The presence of magnesium is consistent with the formation of a magnesium-based compound which is resistant to acid cleaning, such as $MgSiN_2$.[37]

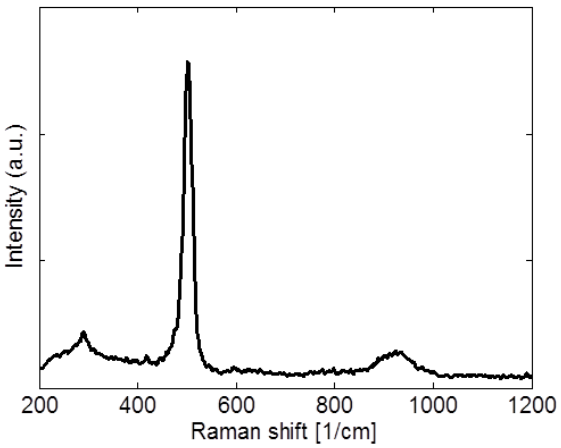

Fig.6 Raman shift of *MSN* frustules

According to the results of the XRD analysis presented in **Fig. 5**B, the *MSN*-frustules consist of silicon and $MgSiN_2$. Rietveld analysis of the crystalline phases, suggests the content of $MgSiN_2$ and Si to be approximately 94% and 6 wt%, respectively. The unit cell parameter of Si, M = 28.09, T = 293 K, refined in the cubic *Fd*-3*m* space group was 5.4316 Å. $MgSiN_2$, M = 80.40, T = 293 K, was refined in the orthorhombic space group *Pna*21, with resulting unit cell parameters a = 5.3651 Å, b = 6.3844 Å and c = 4.9731. The final *Rwp* was 5.67. From visual inspection of the diffractogram, the amorphous phase appears to have disappeared after nitriding. Due to the multitude of reactants and a gradual increase in temperature, some possible side reactions are:

Formation of magnesium nitride:

$$3Mg_{(g)} + 2NH_{3(g)} \rightarrow Mg_3N_{2(s)} + 3H_{2(g)} \quad (5)$$

Formation of elemental silicon:

$$2Mg_{(g)} + SiO_{2(s)} \rightarrow 2MgO_{(s)} + Si_{(s)} \quad (6)$$

Formation of magnesium silicide and magnesium oxide:

$$SiO_{2(s)} + 4Mg_{(s)} \rightarrow 2MgO_{(s)} + Mg_2Si_{(s)} \quad (7)$$

Formation of magnesium silicates:

$$MgO_{(s)} + SiO_{2(s)} \rightarrow MgSiO_{3(s)} \quad (8)$$

$$2MgO_{(s)} + SiO_{2(s)} \rightarrow Mg_2SiO_{4(s)} \quad (9)$$

Formation of silicon oxynitride:

$$3Si_{(s)} + SiO_{2(s)} + 4NH_{3(g)} \rightarrow 2Si_2N_2O_{(s)} + 6H_{2(g)} \quad (10)$$

Formation of silicon nitride:

$$3SiO_{2(s)} + 6Mg_{(g)} + 4NH_{3(g)} \rightarrow Si_3N_{4(s)} + 6MgO_{(s)} + 6H_{2(g)} \quad (11)$$

However, oxygen containing compounds (SiO_2, MgO, $Mg(OH)_2$, $MgSiO_3$ etc.) are surprisingly not detected by XRD despite oxygen being detected by EDS. Pollution of the sample in air is also another possibility for the observation of oxygen in these samples which could explain the failure to detect oxygen containing compounds in XRD. These oxygen containing compounds might also exist in a quasi-amorphous state within the *MSN*-frustules, preventing any diffraction peak from being seen.[38, 39] The absence of compounds other than $MgSiN_2$ and Si indicates that the formation of $MgSiN_2$ is more thermodynamically stable than the formation of silicon nitride and silicon oxynitride for the conditions of this experiment *(cf. eq*. 10-11). The presence of elemental silicon can be explained by the magnesiothermic reduction of silica occurring at temperatures as low as 650 °C.[13] The formation of elemental silicon would thus be favored at temperatures lower than 800 °C. The formation of $MgSiN_2$ at 800 °C follows the decomposition of magnesium nitride (Mg_3N_2) which is formed at lower temperature and acts like a nitrogen sink preventing the formation of other nitrides until the decomposition temperature is reached.[40, 41] The formed Mg_3N_2 then becomes unstable and decomposes at 800 °C, releasing the required nitrogen to form $MgSiN_2$.[42]

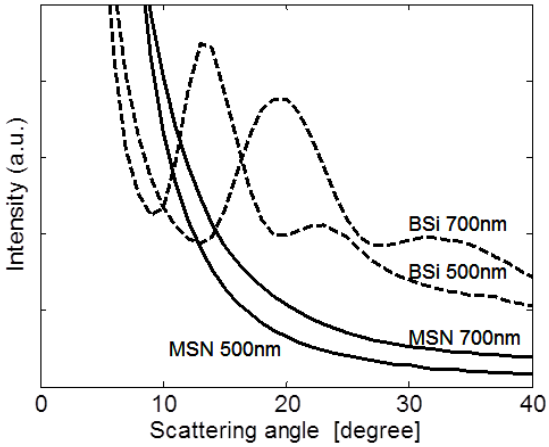

Fig.7 Angular dependence of optical forward scattering of the *BSi* and *MSN* samples carried out at 500 and 700 nm wavelength

Raman spectrum of the *MSN* sample is given in **Fig. 6** and exhibits silicon peaks at 290, ~505 and 930 cm^{-1}. The 505 cm^{-1} transverse optical phonon peak displayed a shift away from 520 cm^{-1} which is expected for bulk silicon. An analysis of Raman images showed that for a majority of the frustule area, the peak was in the range from 505 to 515 cm^{-1}. According to theory on size dependent Raman shift of Si nanocrystals[43] this corresponds to a size of about 2-3 nm. A Raman shift of 480 cm^{-1} is expected from amorphous silicon nanoparticles.[44] This peak is not visible in the spectra.

Optical transmission and luminescence

BSi-frustules exhibits wavelength dependent diffraction (15-20 °) due to the quasi-regular pattern with a periodicity of ~2 µm. Optical diffraction experiments on *MSN* frustules did not display this diffraction effect. The observed surface coarsening may induce a broadening of the diffraction peak and an increased light scattering. Results from optical scattering experiments at 500 and 700 nm wavelengths are displayed in **Fig. 7**. The experiments were carried out with a 2 mm collimated light beam transmitted through a glass plate partly covered by frustules. The coverage was much lower for the *MSN* sample, so the relative scattering intensity of *BSi* and *MSN* cannot be compared. Broad diffraction peaks are clearly observed for the *BSi* sample. For a hexagonal pattern with hole spacing of 2400 nm, the predicted lowest order diffraction peaks are predicted to be 13.3 ° and 23.6 ° for 500 nm and 18.9 ° and 34.1 ° for 700 nm. All of these diffraction peaks are absent for the *MSN* sample.

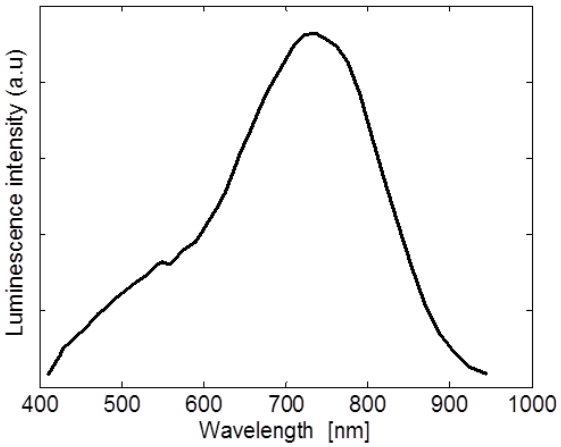

Fig. 8 Luminescence from *MSN* sample with 350 nm excitation.

The surface coarsening is expected to be the main reason for this. Luminescence from the *MSN* sample is presented in **Fig. 8**. The excitation wavelength was 350 nm. Luminescence from undoped MgSiN2 has not been reported in the literature, despite numerous reports on luminescence from doped MgSiN2.[25, 45] We therefore attribute the observed luminescence to originate from nanocrystalline silicon. The luminescence is broadband, which is expected from silicon nanocrystals with variation in crystal size.[46] **Fig. 9** shows the results of light transmission experiments with a hyper-spectral camera. The frustules were distributed on a glass plate, and spectra were averaged over a frustule area and on an area of bare glass plate. The transmittance spectra of the frustules were normalized to the spectra of the bare glass plate. *MSN*-frustules demonstrated a lower transmittance than *BSi* which can be caused by an increased scattering and by an increased absorption. The Si nanocrystals may be responsible for the increased absorption.[47]

Conclusions

Diatom silica frustules have undergone simultaneous metallothermic reduction and nitriding at 800 ^{o}C. The resulting frustule replicas were found to consist of $MgSiN_2$ and nano-crystalline elemental silicon based on SEM, EDS and XRD and Raman analysis. Nano-crystalline elemental silicon was formed by the metallothermic reduction of silica at temperatures lower than 800 ^{o}C. The frustules original micro and nanoscaled morphological features have been well preserved, although an increased surface roughness was observed and attributed to effects of sintering within the material. Wavelength dependent diffraction of light was observed in *BSi*-frustules, but not in *MSN* frustules and is likely caused by the increased surface coarsening observed in *MSN* frustules. *MSN* frustules demonstrated a lower transmittance in comparison with *BSi*-frustules and could be caused by increased scattering and absorption of light. Silicon nanocrystals may be responsible for increased absorption. Luminescence from the silicon nanocrystals was observed. The simultaneous metallothermic reduction and nitriding of diatom frustules is a facile route to synthesize 3D $MgSiN_2$ frustule replicas. A prospective combination of photonic properties arising from these nanostructures and luminescent properties from nanocrystalline Si in an $MgSiN_2$ matrix could contribute to new concepts in light emitting and solar cell technology.

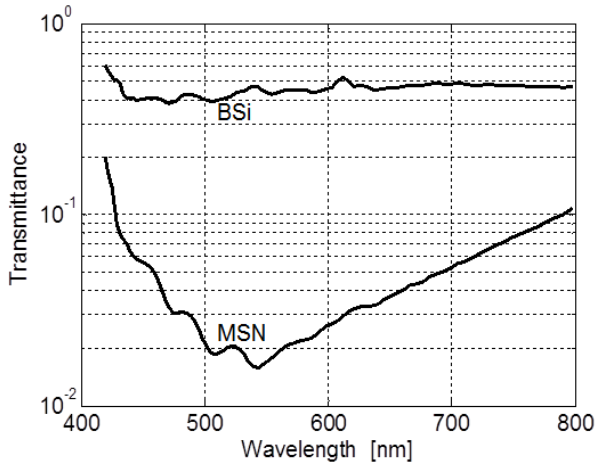

Fig. 9 Optical transmittance of *MSN* and *BSi* frustules.

Acknowledgements

The authors acknowledge the Norwegian Research Council for economic support (contract #10358700)

Notes and references

[a] *Department of Materials Science and Engineering, NTNU, N-7491 Trondheim, Norway*
[b] *SINTEF Materials and Chemistry, N-7465 Trondheim, Norway*
[*] *Corresponding author: Tel: +47 7359 2761; E-mail: gabriella.tranell@ntnu.no*

† Electronic Supplementary Information (ESI) available: Figure 1, Figure 2, Figure 3, Figure 4, Figure 5, XRD Observed-calculated-difference plot. (. See DOI: 10.1039/b000000x/

1. F. E. Round, R. M. Crawford and D. G. Mann, *The Diatoms: Biology & Morphology of the Genera*, Cambridge University Press, 1990.
2. R. Gordon, D. Losic, M. A. Tiffany, S. S. Nagy and F. A. S. Sterrenburg, *Trends in Biotechnology*, 2009, **27**, 116-127.
3. D. Losic, G. Rosengarten, J. G. Mitchell and N. H. Voelcker, *Journal of Nanoscience and Nanotechnology*, 2006, **6**, 982-989.
4. S. A. Crawford, M. J. Higgins, P. Mulvaney and R. Wetherbee, *Journal of Phycology*, 2001, **37**, 543-554.
5. L. De Stefano, P. Maddalena, L. Moretti, I. Rea, I. Rendina, E. De Tommasi, V. Mocella and M. De Stefano, *Superlattices and Microstructures*, 2009, **46**, 84-89.
6. E. De Tommasi, I. Rea, V. Mocella, L. Moretti, M. De Stefano, I. Rendina and L. De Stefano, *Opt. Express*, 2010, **18**, 12203-12212.
7. A. Gogoi, A. K. Buragohain, A. Choudhury and G. A. Ahmed, *Journal of Quantitative Spectroscopy and Radiative Transfer*, 2009, **110**, 1566-1578.
8. L. De Stefano, L. Rotiroti, M. De Stefano, A. Lamberti, S. Lettieri, A. Setaro and P. Maddalena, *Biosensors and Bioelectronics*, 2009, **24**, 1580-1584.
9. H. Jingyun, W. Xudong and W. Zhong Lin, *Nanotechnology*, 2008, **19**, 025602.
10. W. Yang, P. J. Lopez and G. Rosengarten, *Analyst*, 2011, **136**, 42-53.
11. J. Toster, K. S. Iyer, W. Xiang, F. Rosei, L. Spiccia and C. L. Raston, *Nanoscale*, 2013, **5**, 873-876.

12. E. De Tommasi, L. De Stefano, I. Rea, L. Moretti, M. De Stefano and I. Rendina, Strasbourg, France, 2008.
13. Z. Bao, M. R. Weatherspoon, S. Shian, Y. Cai, P. D. Graham, S. M. Allan, G. Ahmad, M. B. Dickerson, B. C. Church, Z. Kang, H. W. Abernathy Iii, C. J. Summers, M. Liu and K. H. Sandhage, *Nature*, 2007, **446**, 172-175.
14. Z. Bao, E. M. Ernst, S. Yoo and K. H. Sandhage, *Advanced Materials*, 2009, **21**, 474-478.
15. Y. Cai, S. M. Allan, K. H. Sandhage and F. M. Zalar, *Journal of the American Ceramic Society*, 2005, **88**, 2005-2010.
16. Y. Cai, M. R. Weatherspoon, E. Ernst, M. S. Haluska, R. L. Snyder and K. H. Sandhage, in *Synthesis and Processing of Nanostructured Materials: Ceramic Engineering and Science Proceedings*, John Wiley & Sons, Inc., 2008, pp. 49-56.
17. S. Dudley, T. Kalem and M. Akinc, *Journal of the American Ceramic Society*, 2006, **89**, 2434-2439.
18. D.-h. Lee, W. Wang, T. Gutu, C. Jeffryes, G. L. Rorrer, J. Jiao and C.-h. Chang, *Journal of Materials Chemistry*, 2008, **18**, 3633-3635.
19. P. J. Lopez, J. Desclés, A. E. Allen and C. Bowler, *Current Opinion in Biotechnology*, 2005, **16**, 180-186.
20. K. H. Sandhage, S. M. Allan, M. B. Dickerson, C. S. Gaddis, S. Shian, M. R. Weatherspoon, Y. Cai, G. Ahmad, M. S. Haluska, R. L. Snyder, R. R. Unocic, F. M. Zalar, Y. Zhang, R. A. Rapp, M. Hildebrand and B. P. Palenik, *International Journal of Applied Ceramic Technology*, 2005, **2**, 317-326.
21. K. Sandhage, *JOM Journal of the Minerals, Metals and Materials Society*, 2010, **62**, 32-43.
22. U. Kusari, Z. Bao, Y. Cai, G. Ahmad, K. H. Sandhage and L. G. Sneddon, *Chemical Communications*, 2007, 1177-1179.
23. *United States Pat.*, 7615206, 2009.
24. I. A. Ødegård, Norwegian University of Science and Tecnology, NTNU, 2012.
25. C. J. Duan, A. C. A. Delsing and H. T. Hintzen, *Journal of Luminescence*, 2009, **129**, 645-649.
26. C. Jeffryes, J. Campbell, H. Li, J. Jiao and G. Rorrer, *Energy & Environmental Science*, 2011, **4**, 3930-3941.
27. Z. Lenčéš, K. Hirao, Y. Yamauchi and S. Kanzaki, *Journal of the American Ceramic Society*, 2003, **86**, 1088-1093.
28. A. A. Borissov, L. D. Luca and A. G. Merzhanov, *Self-propagating high-temperature synthesis of materials*, Taylor & Francis, 2002.
29. K. Umemura, Y. Noguchi, T. Ichinose, Y. Hirose and S. Mayama, *Journal of Nanoscience and Nanotechnology*, 2010, **10**, 5220-5224.
30. H. Uchida, K. Itatani, M. Aizawa, F. S. Howell and A. Kishioka, *Advanced Powder Technology*, 1999, **10**, 133-143.
31. B. W. Jong, G. J. Slavens and D. E. Traut, *Journal of Materials Science*, 1992, **27**, 6086-6090.
32. J. Ma, M. Wu, Y. Du, S. Chen, G. Li and J. Hu, *Journal of Alloys and Compounds*, 2009, **476**, 603-605.
33. G. R. Hasle and C. B. Lange, *Diatom Research*, 1992, **7**, 37-68.
34. M. G. A. P. Setty, *Micropaleontology*, 1966, **12**, 511-514.
35. Y.-J. S. Park, In-Hyuck ; Kim, Hai-Doo, *Journal of the Korean Ceramic Society*, 2008, **45**, 675-680.
36. J.-F. Yang, T. Ohji, S. Kanzaki, A. Díaz and S. Hampshire, *Journal of the American Ceramic Society*, 2002, **85**, 1512-1516.
37. R. G. Blair, A. Anderson and R. B. Kaner, *Chemistry of Materials*, 2005, **17**, 2155-2161.
38. T. Jäschke and M. Jansen, *Comptes Rendus Chimie*, 2004, **7**, 471-482.
39. B. D. Cullity and S. R. Stock, *Elements of x-ray diffraction*, Prentice Hall, 2001.
40. D.-W. Kim, T.-H. Kim, H.-W. Park and D.-W. Park, *Applied Surface Science*, 2011, **257**, 5375-5379.
41. F. Zong, C. Meng, Z. Guo, F. Ji, H. Xiao, X. Zhang, J. Ma and H. Ma, *Journal of Alloys and Compounds*, 2010, **508**, 172-176.
42. G. H. Aylward and T. J. V. Findlay, *SI Chemical Data*, John Wiley & Sons Australia, 2007.
43. S. K. Gupta and P. K. Jha, *Solid State Communications*, 2009, **149**, 1989-1992.
44. O. Debieu, R. P. Nalini, J. Cardin, X. Portier, J. Perriere and F. Gourbilleau, *Nanoscale Res Lett*, 2013, **8**, 31.
45. C. Kulshreshtha, J. H. Kwak, Y.-J. Park and K.-S. Sohn, *Opt. Lett.*, 2009, **34**, 794-796.
46. S. Mirabella, R. Agosta, G. Franzò, I. Crupi, M. Miritello, R. Lo Savio, M. A. Di Stefano, S. Di Marco, F. Simone and A. Terrasi, *Journal of Applied Physics*, 2009, **106**, -.
47. S. Dhara and P. Giri, *Nanoscale Res Lett*, 2011, **6**, 320.